

High ZT of new half-Heusler LiXZ (X=La, Y and Z=Ge, Si) alloys at room temperature



Hamid Missoum^a, Khedija Talbi^a, Friha Khelfaoui^b, Bachir Bouhadef^a, Ali Mir^a, Youcef Cherchab^{a,c}, Rafael González-Hernández^d, Y. Al-Douri^{e,f,*}

^a Department of Physics, University of Relizane, Ahmed Zabana, Po Box 048000, Bormadja, Relizane, Algeria

^b Laboratory of Physicochemical Studies, University of Saida, Dr. Moulay Tahar, Saida, 20000, Algeria

^c Laboratoire de Microphysique et de Nanophysique (LaMIN), ENPO, Po Box 1523 EL M'Naouer, Oran, 31000, Algeria

^d Department of Physics, Universidad del Norte, Po Box 080001, Barranquilla, Colombia

^e Department of Mechanical Engineering, Faculty of Engineering, Piri Reis University, Eflatun Sk. No:8, 34940, Tuzla, Istanbul, Turkey

^f Nanotechnology and Catalysis Research Centre, University of Malaya, 50603, Kuala Lumpur, Malaysia

ARTICLE INFO

Keywords:

DFT
Half-Heusler
Thermoelectric
Electronic
Mechanical

ABSTRACT

The thermoelectric, electronic and structural properties of novel half-Heusler (HH) LiXZ ($X = La, Y; Z = Ge, Si$) alloys are researched using the full-potential linearized augmented plane wave (FP-LAPW) method and semi-classical Boltzmann transport theory under the constant time relaxation. Our results reveal that all alloy can be experimentally synthesized due to they have exhibited energetic, mechanical and dynamic stability. In addition, all these systems present semiconducting behaviour with a flatness band near Fermi energy (E_F) level, which makes its favourable for thermoelectric compounds. The calculated thermoelectric properties show that LiLaZ is highest p-type thermo power. However, LiYZ is highest n-type thermo power performance. The Seebeck coefficients are higher than at room temperature of thermoelectric Bi₂Te₃. The conductivity is considerably low of LaLiGe and LiYSi. The higher values of figure of merit (ZT) and power factor of LiXZ half-Heusler alloys make them promising for high-performance thermoelectric applications resulting from the favourable features of their band structure and high mechanical stability.

1. Introduction

The most progress of thermoelectric applications, providing a comprehensive review of different aspects; cooling/heating [1], thermoelectric generator (TEG) [2,3], heat flux sensor [4] and material industry [5]. The better thermoelectric properties for a long time chosen by most companies for commercial applications are bismuth telluride (Bi₂Te₃) and its alloys with a highest figure of merit (ZT), about 1 [6], lead telluride (PbTe) that is used at higher temperatures up to 900 K [7]. The mainly problem is a wide lattice thermal conductivity, so nano-block structuring [8] is considered as an effective way to improve the thermoelectric properties by reducing the lattice thermal conductivity [9]. Half-Heusler (HH) alloys have been attracting extensive research interest over the last two decades. Generally, for n-as well as for p-type Half-Heusler alloys, most ZTs at 300 K are below 0.3. Above 300 K, many peak ZTs are below 1 but can reach 1.6 [10]. Whereas the most successful system for the n-type is (Ti, Zr, Hf) NiSn-system with Sb/Sn

substitution, for p-type, it is the (V, Nb, Ta) FeSb-system doped with Ti, Zr or Hf [11–16]. Various groups used additions, mainly nanoparticles, to reduce the thermal conductivity for enhancing ZT [17–20]. Chauhan et al. [21] have achieved a better result by mixing ZnO with ZrNiSn with ZT ~ 1. To enhanced the ZT via a drastic reduction of thermal conductivity, Rogl et al. [22,23] have investigated the influence of severe plastic deformation via high-pressure torsion. 8-electron half-Heusler alloys is another class, which ZT is close to 1, The experience shows that using metallic phase nano inclusions as dopants by varying the valence electron count to enhance the Seebeck coefficient [11]. Vikram et al. [24] have calculated ZT = 1.37 for RbPBa and ZT = 1.56 for AgPMg. While, Hoat et al. [25] and Ciftci et al. [26] have showed that KScX (X = C and Ge) half-Heusler alloys are considered thermoelectric efficient materials, which is 1.5 times higher than Bi₂Te₂ at room temperature. Therefore, it is not available in the literature any data for ZTs using DFT calculations. In addition, Kieven et al. [27] have selected Li-based half-Heusler (LiCuS and LiZnP) alloys as a potential buffer layer

* Corresponding author. Department of Mechanical Engineering, Faculty of Engineering, Piri Reis University, Eflatun Sk. No:8, 34940, Tuzla, Istanbul, Turkey.
E-mail address: yaldouri@yahoo.com (Y. Al-Douri).

Table 1

Atomic positions for the three structural configurations; type 1 (α), type 2 (β) and type 3 (γ).

	Li _{position}	X _{position(X = Y,La)}	Z _{position(Z = Ge,Si)}
Type 1	$4b\left(\frac{1}{2}, \frac{1}{2}, \frac{1}{2}\right)$	$4a(0,0,0)$	$4c\left(\frac{1}{4}, \frac{1}{4}, \frac{1}{4}\right)$
Type 2	$4a(0,0,0)$	$4c\left(\frac{1}{4}, \frac{1}{4}, \frac{1}{4}\right)$	$4b\left(\frac{1}{2}, \frac{1}{2}, \frac{1}{2}\right)$
Type 3	$4c\left(\frac{1}{4}, \frac{1}{4}, \frac{1}{4}\right)$	$4b\left(\frac{1}{2}, \frac{1}{2}, \frac{1}{2}\right)$	$4a(0,0,0)$

for optoelectronics. In the light of these studies, we have drawn inspiration for conducting our research. We have chosen the half-Heusler (LiXZ), taking X = La and Y; Z = Ge and Si. The motivation of our choice is the resemblance of physical properties to those obtained for LiScSi [28], XScZ (X = K, Na, Li; Z = Ge, Si, C) [29] and Li-based half-Heusler (Z = Si, Ge, Bi, Sb, As; Y = Sc, Be; X = Li) alloys [30], all have eight-valence electron half-Heusler alloys. On another hand, Kamlesh et al. [29] have demonstrated the resemblance between LiScGe (LiScSi) and KScGe (KScSi) and confirmed their dynamic stability by phonon band dispersion. Many thermoelectric materials are being explored for power generation applications such as GeTe [31], Bi₂Te₃ [32], PbTe [33,34] and half-Heusler compounds [35].

This work investigates the thermoelectric, electronic and structural properties of half-Heusler LiXZ (Z = Si, Ge; X = Y, La) alloys utilising the full-potential linearized augmented plane wave (FP-LAPW) method [36] within density functional theory (DFT) [37] and semi classical Boltzmann transport theory [38]. Furthermore, the ground state properties, such as the lattice parameter, bulk modulus cohesive energy and formation enthalpy, are calculated using the generalized gradient approximation (GGA) [39]. The structural stability is also checked via the calculation of elastic constants. Additionally, for a good estimation of energy bandgap related to experimental data, we have employed the modified Beck-Johnson exchange (mBJ) potential [40,41]. The present work of half-Heusler LiXZ alloys contributes to estimating their potential as good thermoelectric materials and provides a guidance to the experimentalist to produce these new half-Heusler alloys. Therefore, it is not available in the literature any data for our calculated equilibrium parameters. This paper is organized as follows; section 2 presents the computational details. While, section 3 is devoted to the results and discussion. Finally, the conclusions are outlined in section 4.

2. Computational

The thermoelectric, electronic and mechanical properties of half-Heusler LiXZ (X = La, Y and Z = Ge, Si) alloys are researched in framework of density functional theory (DFT) implemented in Wien2k package [36]. The exchange-correlation potential is considered within PBE-GGA parameterization [39]. In addition, the Tran-Blaha modified Becke-Johnson exchange (mBJ) potential, which depends solely on semi-local quantities, is employed in combination with the PBE correlation to reach an accurate bandgap [40–42]. These results have been confirmed with the HSE approach. Maximum value of wave functions expansion inside the spheres is fixed at $l_{max} = 10$. The plane wave cutoff takes the value $k_{max} = 9/R_{MT}$ where R_{MT} is smallest value of atomic sphere radii inside the cell, while $G_{max} = 14Ry^{(1/2)}$ is maximum Fourier expansion of charge density with $17 \times 17 \times 17$ Monkhorst-Pack mesh points [43]. We have selected a charge convergence, 0.0001e and energy convergence, 0.00001 Ryd during self-consistency cycles.

The thermal transport properties are calculated using the semi-classical Boltzmann transport theory [38] as implemented in BoltzTrap code [44]. We have calculated the transport properties, including the Seebeck coefficient (S), electrical conductivity (σ), electronic thermal conductivity (κ_e) and power factor (PF), as a function of chemical potential, carrier concentration and temperature using a dense k point with $43 \times 43 \times 43$ Monkhorst-Pack mesh. The phonon dispersion curves are obtained by using Phonopy code [45] within fast Fourier transformation of real-space interatomic force constant matrix obtained through dynamical matrices calculated for the $5 \times 5 \times 5$ q-mesh point grid.

3. Results and discussion

3.1. Structural properties

The results of structural calculation of half-Heusler (HH) LiXZ (X = La, Y, and Y=Ge, Si) alloys are displayed in Table 1. There are three configurations α , β and γ for Li-based XYZ half-Heusler alloys, as illustrated in Fig. 1. For the α -type, Li, X and Z atoms are located at $4b$ (1/2, 1/2, 1/2), $4c$ (1/4, 1/4, 1/4) and $4a$ (0,0,0) Wyckoff positions, respectively. The β and γ phases are just the exchange of $4a$ and $4c$ (4b and 4c) occupation sites, respectively. Table 1 presents all positions. Fig. 2 shows that phase α has a stable ground state than phases β and γ in LiXZ alloys. The Murnaghan's equation of state [46] is fitted to E (V) curves to determine the parameters of equilibrium, like cohesive energy (E_{coh}), bulk modulus (β) and ground-state parameters (a_0) of LiXZ HH alloys. The results show that lattice constant (a_0) decreases accompanied by an

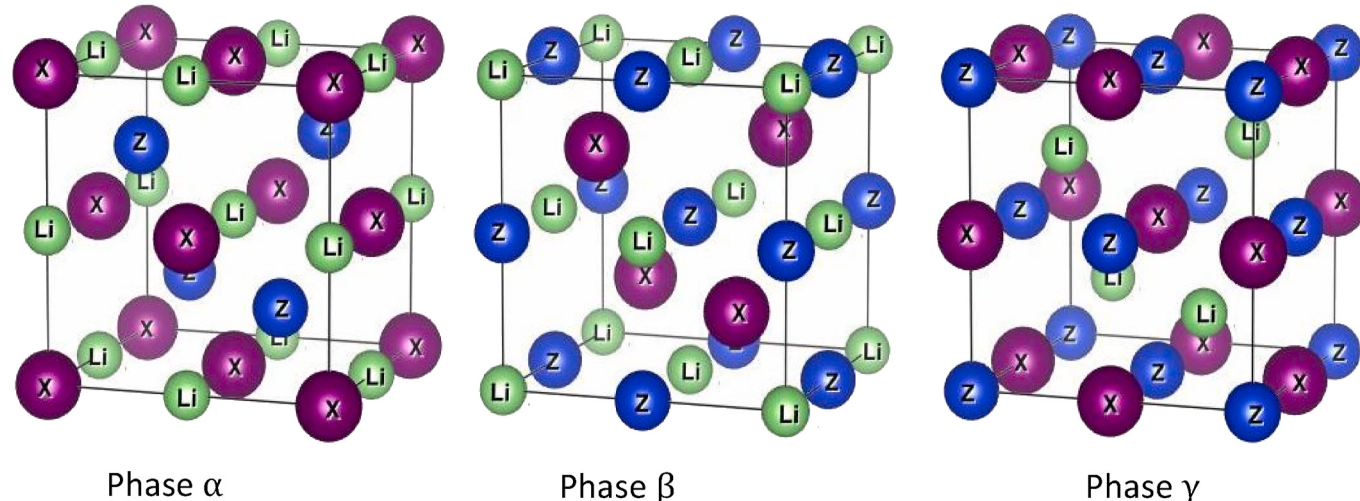


Fig. 1. Crystal structure of LiXZ (X = La, Y and Z = Ge, Si) in three different phases; α , β and γ . In cubic MgAgAs structure with a space group F-43m (No. 216) (C1b).

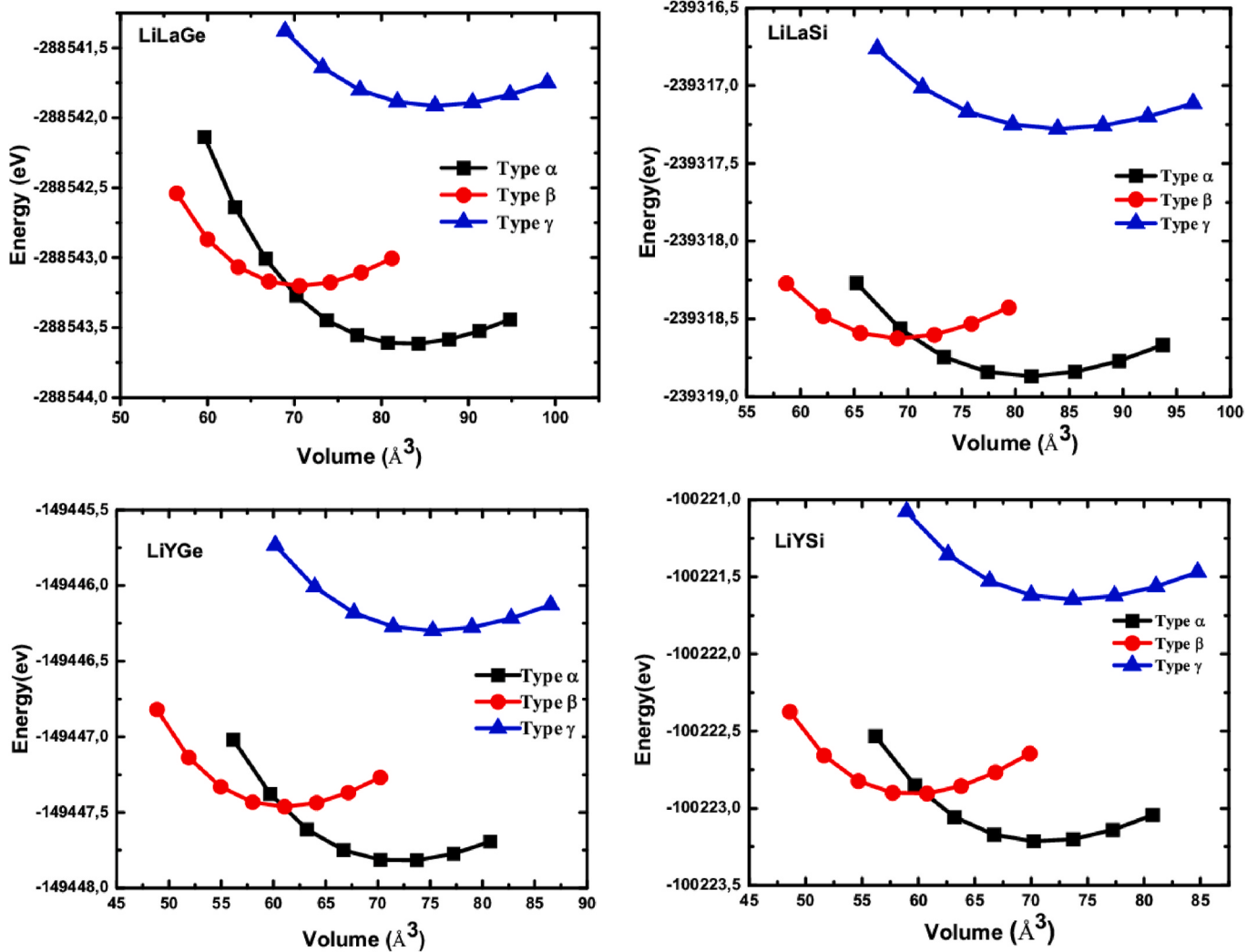


Fig. 2. Total energy versus volume of LiXZ (X = La, Y and Z = Ge, Si) in three phases.

Table 2
Minimum Energy stability of three types of half-Heusler LiXZ alloys.

Minimum Energy	Types			
		Type 1	Type 2	Type 3
LiLaGe	E _{tot} (ev)	-288543.62	-288542.06	-288543.36
LiLaSi	E _{tot} (ev)	-239318.98	-239317.39	-239318.63
LiYGe	E _{tot} (ev)	-149447.82	-149446.35	-149447.47
LiYSi	E _{tot} (ev)	-100223.22	-100221.70	-100222.92

increasing in the bulk modulus (β) by changing Z element. We have concluded that LiXZ HH alloys became rougher on going from LiLaGe to LiYSi and heavier alloys are more compressible than lighter compounds; the same conclusion is seen in Ref. [29].

From Table 2, we can observe that these alloys have almost the same cohesive energy with a negative sign, which give the impression that are stable from the first moment. Additionally, the formation enthalpies are calculated to examine the stability of our alloys, which reflects the ability. We have calculated the energy of formation per atom of LiXZ using the following [47]:

$$\Delta H_{for}^{LiXZ} = \frac{[E_{tot}^{LiXZ} - (E_{tot}^{Li} + E_{tot}^X + E_{tot}^Z)]}{3} \quad (1)$$

where E_{tot}^{LiXZ} is total energy of HH alloy, whereas E_{tot}^{Li} , E_{tot}^X and E_{tot}^Z are

Table 3
Structural and elastic parameters of half-Heusler LiXZ alloys.

Materials	LiLaGe	LiLaSi	LiYGe	LiYSi
a (Å)	6.93	6.88	6.61	6.57
B(Gpa)	42.25	42.55	48.21	49.28
E _{Coh} (eV/atom)	-3.46	-3.74	-3.63	-3.93
ΔH _{form} (eV/atom)	-1.18	-0.89	-0.77	-0.49
C ₁₁ (Gpa)	75.33	89.09	95.03	99.45
C ₁₂ (Gpa)	26.56	20.39	25.55	25.19
C ₄₄ (Gpa)	9.17	18.07	18.89	18.52
B _H	42.83	43.29	48.71	49.94
G _H (Gpa)	13.77	23.44	24.14	24.56
Y _H (Gpa)	37.28	59.56	62.14	63.31
ν	0.354	0.270	0.287	0.288
B/G	3.11	1.85	2.02	2.03
ν ^s (Km/s)	1.78	2.57	2.49	3.25
ν ^l (Km/s)	3.75	4.59	4.57	3.37
ν ^m (Km/s)	1.99	2.86	2.78	3.25
Θ _D (K°)	196.56	283.49	287.06	336.764
T _m (300°K)	998.19	1079.52	1114.64	1140.75
A (Ws ³ m ⁻⁴)	0.27 10 ⁻⁷	0.330 ⁻⁷	0.3110 ⁻⁷	0.0510 ⁻⁷
Γ	2.17	1.61	1.65	-0.37
γ ²	4.70	2.6	2.7	0.137

ground state energies of lithium (Li), X atoms (lanthanum and yttrium) and Z atoms (germanium and silicon), respectively. The formation energy results are presented in Table 2. The formation energy values are all

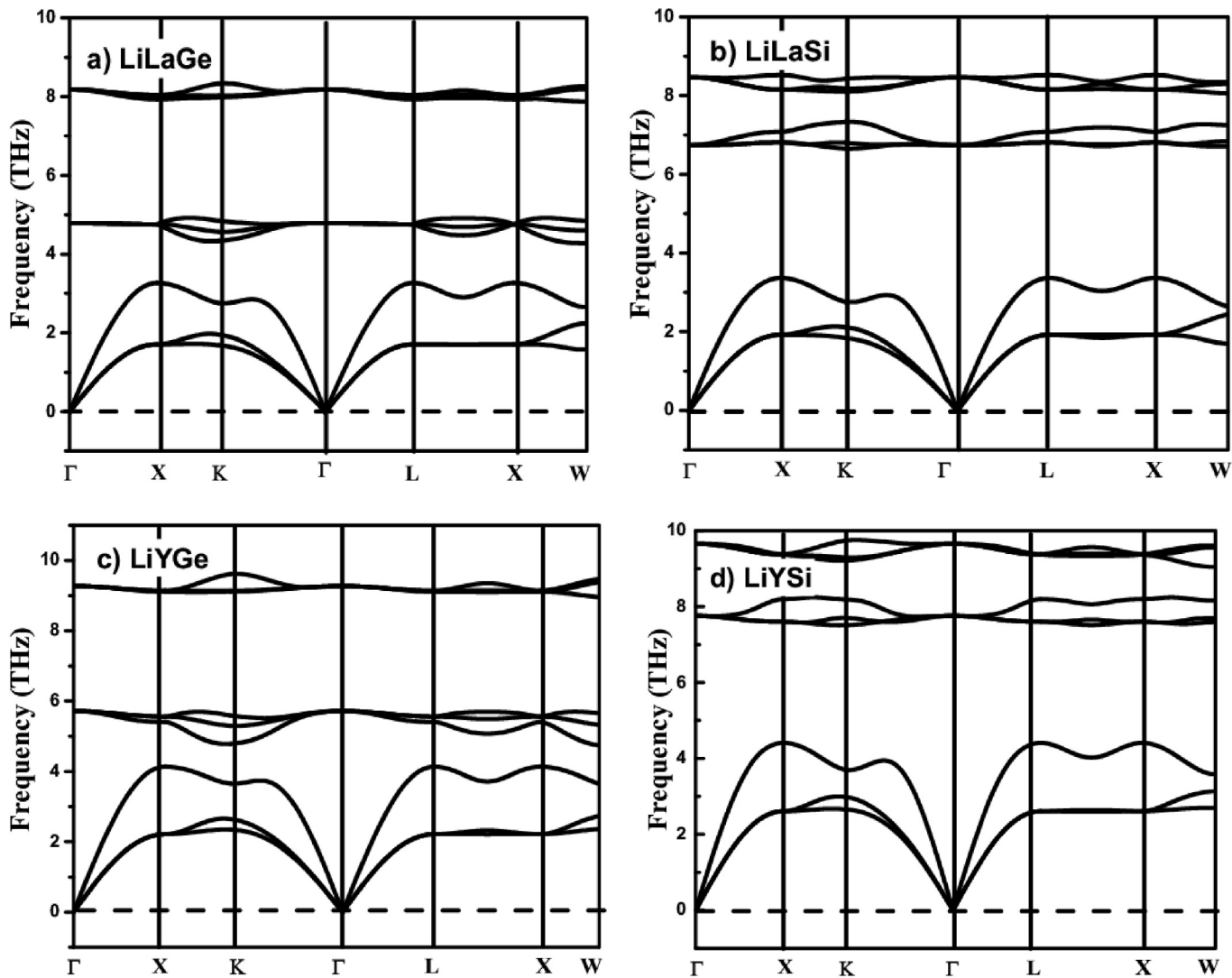


Fig. 3. Phonon dispersion curves for half-Heusler (a) LiLaGe, (b) LiLaSi, (c) LiYGe and (d) LiYSi alloys.

negative, confirming the thermodynamic stability thus; these compounds are stable, indicating the possibility of existing in nature. Since the negative formation energy of LiYSi, LiYGe, LiLaSi and LiLaGe alloys gradually increases, it can be concluded that LiLaGe has the strongest energetic stability. These cohesive energy and formation enthalpy results imply structural stability in this phase and suggest that they can be prepared and stabilized experimentally under normal conditions. There are no data in the literature for our calculated equilibrium parameters.

3.2. Mechanical and dynamical properties

The calculated values of elastic constants of LiXZ ($X = \text{La, Y, and Ge, Si}$) HH alloys are given in **Table 3**. We have used the cubic code [48], developed for cubic symmetry systems, to calculate the three independent elastic constants C_{11} , C_{12} and C_{44} . The average bulk modulus of cubic lattice is calculated using $B = \frac{1}{3}(C_{11} + 2C_{12})$. From **Tables 3** and it is noted that C_{11} , C_{12} , and C_{44} values decrease going from LiYSi, LiYGe, LiLaSi, and LiLaGe, respectively. In this sequence, the results show that LiXZ alloys reduce the bond lengths and increase the cohesive energies. Moreover, the mechanical properties of LiXZ are checked via applying the mechanical stability criteria of cubic crystals [49]:

$$C_{11} - C_{12} > 0, C_{11} > 0, C_{44} > 0, C_{11} + 2C_{12} > 0 \text{ and } B = \frac{1}{3}(C_{11} + 2C_{12}). \quad (2)$$

The calculated elastic constants are displayed in **Table 3** to fulfil all mentioned criteria indicating that LiXZ is elastically stable. Knowledge of the elastic constants yields further information about half-Heusler LiXZ alloys, such as bulk and shear modulus, Young's modulus, and Poisson's ratio. All these quantities are collected in **Table 3**. The arithmetical mean of B_V (Voigt's bulk modulus) [50], B_R (Reuss's bulk modulus) [51], defined bulk modulus B_H , B_V and B_R are extremity limits of B_H . A similar approach is applied to the shear modulus G_H as the bulk modulus B_H . From **Table 3**, the higher values of B_H and G_H are observed in half-Heusler LiYSi alloy due to their short bond length. The B_H values of LiXZ alloys are greater than those of G_H , in this regard, LiXZ alloys are more inflexible to uniaxial straining than to lateral contraction [52]. The shear modulus G_H has the same trends as C_{44} . Via B_H and G_H , the calculation of Young's modulus (Y) and Poisson's ratio are possible using [53].

$$Y = \frac{9BG}{3B + G} \quad (3)$$

$$\nu = \frac{1}{2} \left(\frac{B - (2/3)G}{B + (1/2)G} \right) \quad (4)$$

Table 4

The direct and indirect bandgaps of LiXZ calculated with two different approaches MBJ and HSE.

MATERIAL	MBJ (eV)	HSE (eV)
LiYGe Direct bandgap	0.974	0.969
LiYSi Direct bandgap	0.878	0.875
LiLaGe indirect bandgap	0.804	0.845
LiLaSi indirect bandgap	0.704	0.690

The results of Younng's modulus are depicted in [Table 3](#). All values obtained for B/G ratio suggested by Pugh's [54] are higher than extreme limit of ductile regime (≥ 1.75). From [Tables 3](#) and it is higher than 0.25, it suggests that LiXZ half-Heusler has further ionic character according to bonding force types [55]. The values of ν_m concord with those in $A^I B^{III} C^{IV}$ half-Heusler group [30,52,56,57]. The Debye temperature (θ_D) is expressed as [58]:

$$\theta_D = (h / k_B) \left[\left(\frac{3n}{4\pi} \right) (N_A \rho / M) \right]^{\frac{1}{3}} \cdot \nu_m \quad (5)$$

where ρ , M , h , N_A , n and k_B are mass density, molecular weight of the primitive cell, Planck constant, Avogadro's number, number of atoms in primitive cell and Boltzmann's constant, respectively. ν_m denotes average wave velocity, which is defined by the following equation [58]:

$$\nu_m = \frac{1}{3} \left(\frac{1}{v_s^3} + \frac{1}{v_l^3} \right)^{-\frac{1}{3}} \quad (6)$$

$$\text{with } v_s = \sqrt{\frac{3B + 4G}{\rho}} \quad (7) \text{ and } v_l = \sqrt{\frac{G}{\rho}} \quad (7)$$

The results of ν_l (compressional velocity), v_s (sound velocity), ν_m (average sound velocity) and θ_D (Debye temperature) of half-Heusler LiXZ alloys are summarized in [Table 3](#). The value ν_m of LiYSi is significantly greater than LiYGe, LiLaSi, and LiLaGe. The Debye temperature θ_D (K) and melting temperature T_m (K) show the same tendency as ν_m . The results are in agreement with those found in $A^I B^{III} C^{IV}$ half-Heusler alloys [30,52,57]. In addition, the dynamic stability of half-Heusler LiXY (X = La,Y and Z = Ge,Si) alloys is confirmed by calculating the

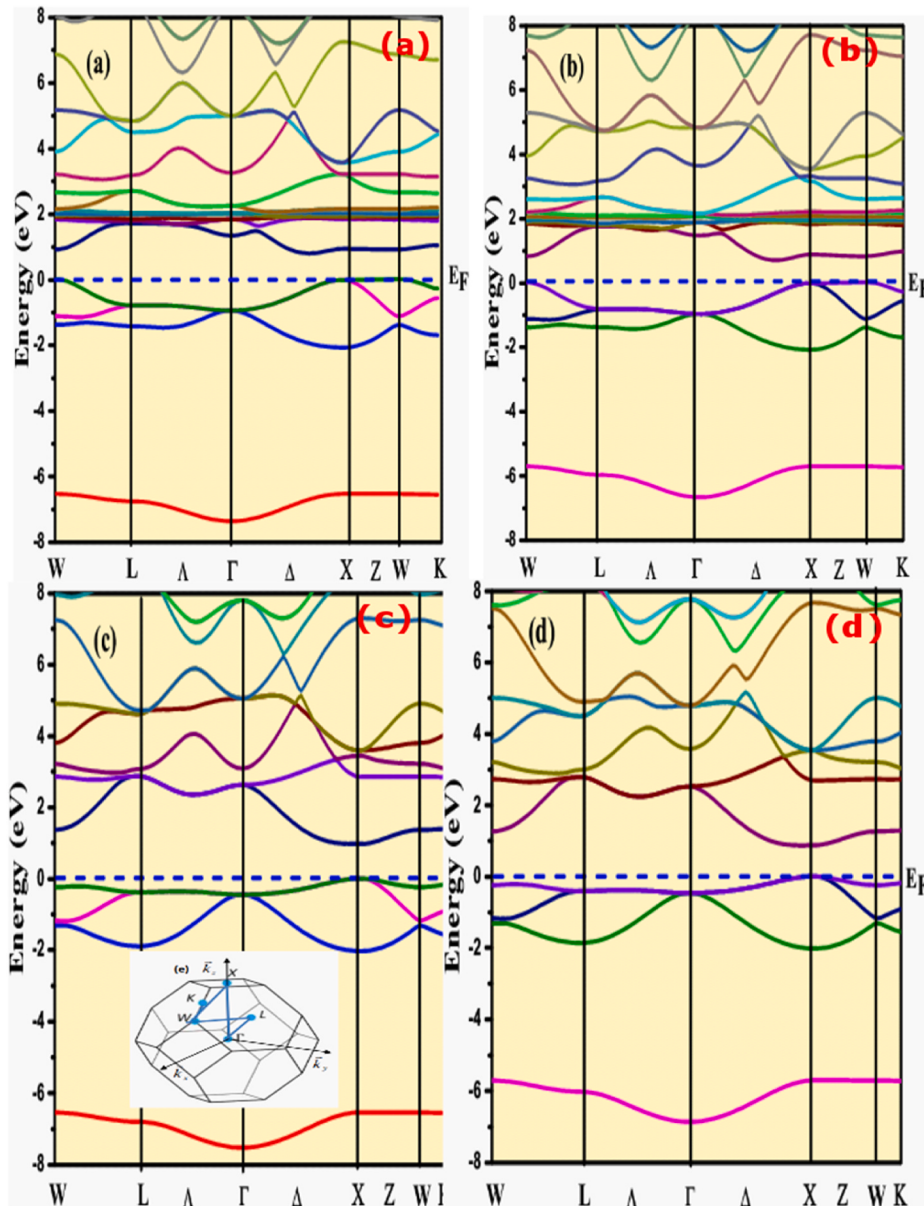


Fig. 4. Electronic band structures of half-Heusler a) LiLaGe,b) LiLaSi c) LiYGe d) LiYSi alloys including first Brillouin Zone with high symmetry points are marked.

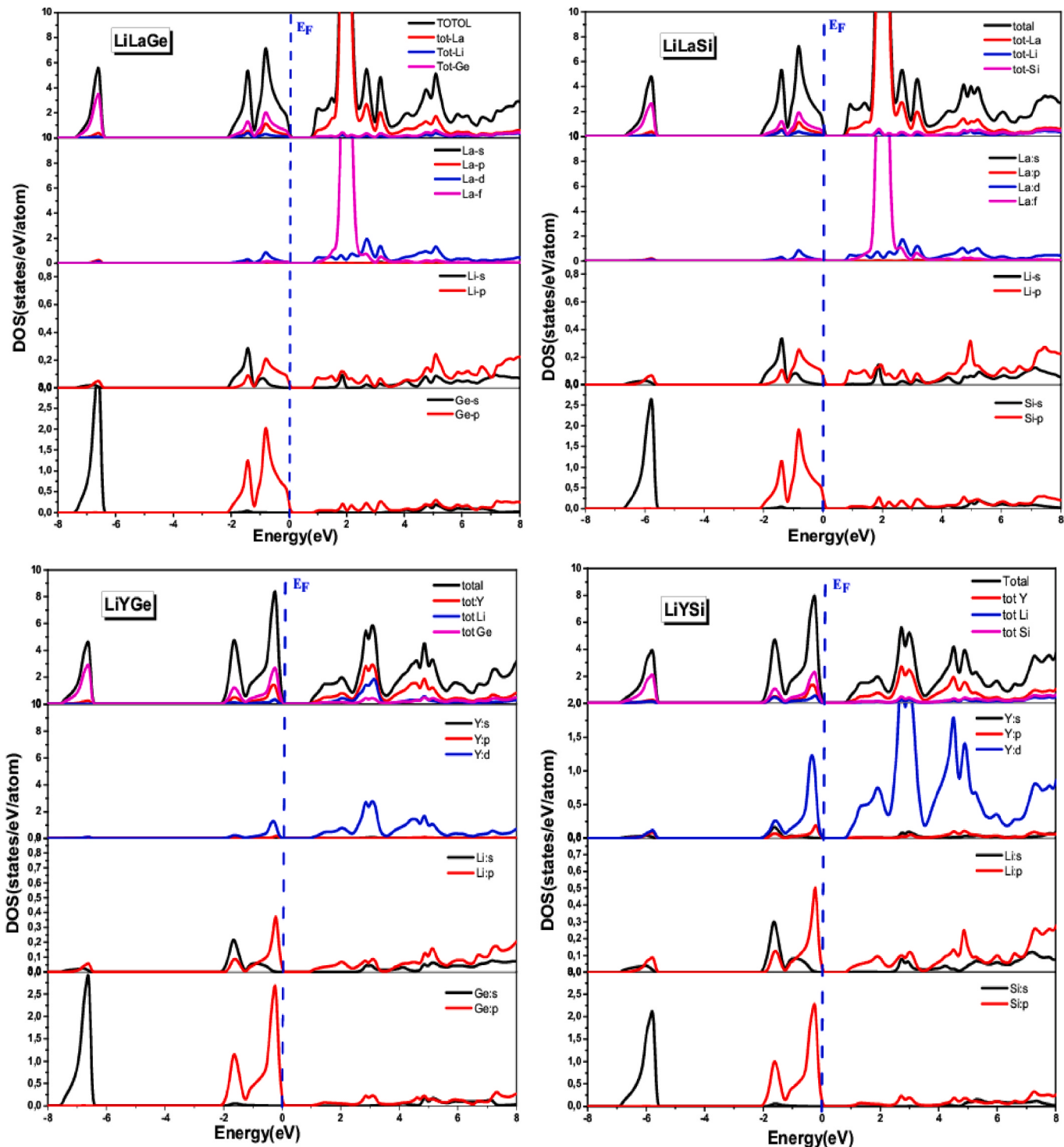


Fig. 5. Total and partial DOS of half-Heusler LiXZ ($X = La, Y$ and $Z = Ge, Si$) alloys.

phonon dispersion curve employing the Phonopy code [45]. In Fig. 3, the obtained phonon dispersion curve along Γ -X-K- Γ -L-X-W in the first Brillouin zone is displayed. From Fig. 3, we have found positive frequencies for the phonon dispersion curves of LiXY alloys; hence, there are no imaginary modes. This indicates that half-Heusler LiXZ alloys are dynamically stable. All these compounds have three atoms in their primitive cell, which generate 9 vibrational modes; 3 acoustic and 6 optical modes. Due to a strong dispersion of acoustic modes and high group velocities, the maximum involvement in heat transfer derives from the acoustic modes [29], and the maximum acoustic frequencies

are found at approximately 3.26 THz (108.72 cm^{-1}), 3.41 THz (113.72 cm^{-1}), 4.15 THz (138.40 cm^{-1}) and 4.0 THz (146.74 cm^{-1}) for LiLaGe, LiLaSi, LiYGe, and LiYSi alloys, respectively. This is consistent with other half-Heusler alloys that present an acoustic frequency of approximately 100 cm^{-1} [59]. We also have no overlap between the acoustic and optical branches, and this phonon bandgap is enlarged from LiYGe, LiLaGe, LiLaSi and LiYSi alloys, respectively. The same behaviour has been reported for LiScZ ($Z = C, Si \& Ge$) [29] and LiScSi [28] alloys. We conclude that LiXY (with $X = La, Y$ and $Z = Ge, Si$) fulfils all criteria of mechanical and dynamical stability.

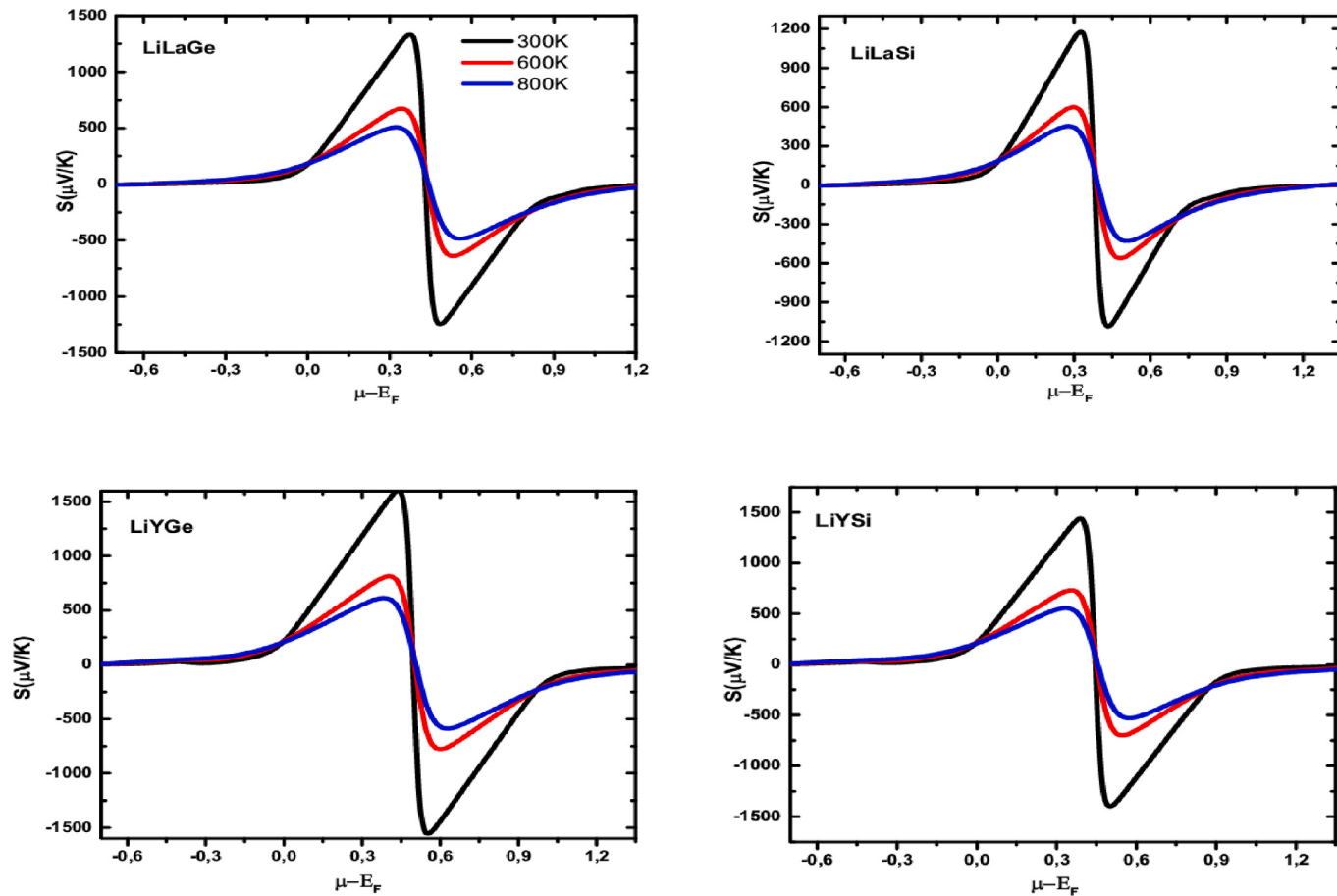


Fig. 6. Seebeck coefficient (S) of half-Heusler LiXZ alloys calculated at different temperatures.

3.3. Electronic properties

The electronic properties of LiXZ ($X = \text{La}, \text{Y}$, and $\text{Y}=\text{Ge}, \text{Si}$) half-Heusler (HH) alloys are investigated by employing mBJ method as compared with HSE approach [41]. The calculations are performed using self-consistent scalar relativistic band gaps with lattice constants (Table 4) and a α -type equilibrium configuration. Fig. 4 shows the band structures of LiXZ HH alloys, and Fermi level is set at zero eV. The electronic band structure is calculated in high symmetry directions in the first Brillouin zone $\text{W-L}-\Gamma-\text{X}-\text{W-K}$. From Fig. 4, the band structures of LiXZ alloys for the same X atoms are very similar. In fact, for $X = \text{La}$ atom, we identify an indirect energy bandgap ($\Gamma-\Delta$), with flatness occurring at the top of valence and bottom conduction bands. For $X = \text{Y}$ atom, the band structure in the vicinity of band edges is located at point X , demonstrating a direct behaviour of bandgap with no flatter band in valence and conduction bands. The Brillouin zone of electronic calculation is shown in Fig. 4. We have observed that the band structures of LiLaGe and LiLaSi alloys are displayed in Fig. 4, show that the VBM has twofold degeneracy in the direction $\text{L}-\Gamma-\text{X}$. Additionally, the CBM has twofold degeneracy in the direction $\text{L}-\Gamma$. The flatness and hence the large effective masses of charge carriers will give rise to high thermopower, as reported in Li-based half-Heusler ($X = \text{Li}$; $\text{Y} = \text{Be}, \text{Sc}$; $Z = \text{As}, \text{Sb}, \text{Bi}$, Ge, Si) alloys [30]. Furthermore, the minimum of band conduction is characterized by band f derived of atom La, which leads to downshifting of CBM of LiLaSi and LiLaGe . The flatter band observed in the conduction band maximum of LiLaSi and LiLaGe , implies a large effective mass and suggests a critical factor to improve the power factor (PF). The direct bandgap is 0.974 eV (0.878 eV) for LiYGe (LiYSi), and the indirect bandgap is 0.804 eV (0.704 eV) for LiLaGe (LiLaSi), which leads to the semiconducting behaviour of LiXZ half Heusler. These

values are compared with HSE approximations (see Table 2).

To the best of our knowledge, these half-Heusler alloys have not been investigated previously, nevertheless, there are no available data that confront the current results but a signified comparison with bandgap I-III-IV half-Heusler alloys is possible, like K-based half-Heusler [26,52, 57] and Li-based half-Heusler [29,30] alloys. Our calculated direct bandgaps are slightly higher than those predicted by Amudhavalli et al. [30], 0.919 eV for LiScGe and 0.782 eV for LiScSi . However, our obtained results are in accord with those reported by Naseri et al. [52], in addition to 0.852 eV (0.921 eV) for KYGe (KYSn) and 0.81 eV for KLaX ($X = \text{Ge}$ and Si) reported by Cherchab et al. [57]. However, the bandgaps are affected by spin-orbit coupling (SOC), which is suspected to downshift the fundamental bandgap [25]. The total and partial densities of states (TDOS and PDOS) are calculated by mBJ potential as shown in Fig. 5, which shows that the top of valence band in the vicinity of E_F is sharpened in two groups of peaks. The first group near the top of VBM comes from the hybridization between combination of d-orbitals of X atoms ($X = \text{La}$ and Y) and p-orbitals of Z atoms ($Z = \text{Si}$ and Ge). The strong character is attributed to p-d hybridization, and opposite trend is found in K-based half-Heusler alloys like KLaGe and KLaSi [52]. The second lower group of peaks is due to same orbitals. We have observed a weak contribution, p(s) orbitals of Li atom in the first (second) groups in all cases. For $X = \text{La}$, the conduction band bottom (CB) above E_F is split into two sub bands, both from atom La as shown in Fig. 5. The higher band is characterized by a very strong band f, while the lower band consists of band d. However, we have observed reversed contributions from orbitals f and d in KLaGe [52]. For $X = \text{Y}$, we have d-band contribution of yttrium (Y) in the whole band conduction, with visible participation of Li orbitals in LiYGe alloy, and a similar trend is found for LiScZ (with $Z = \text{Si}$ and Ge) alloys [57].

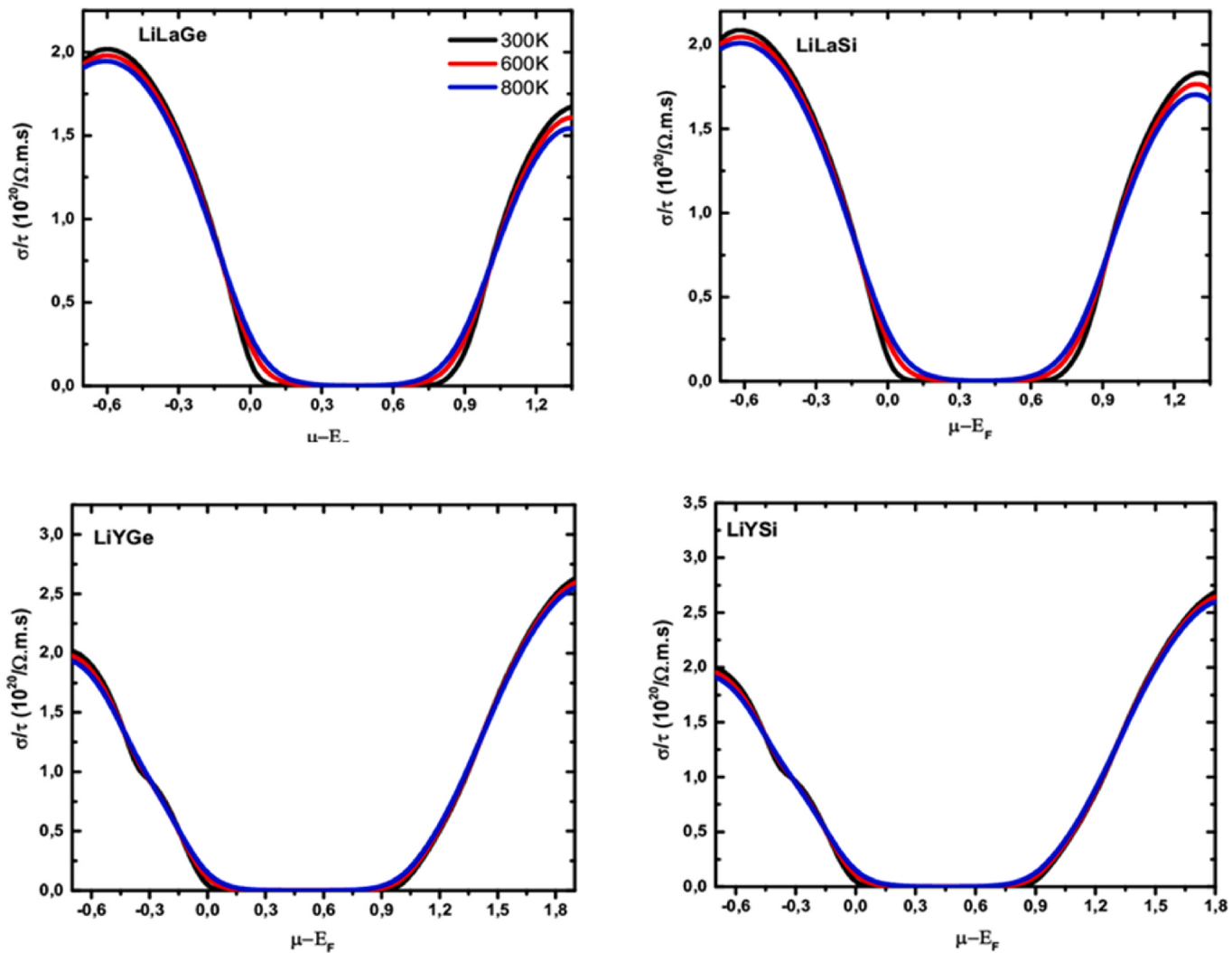


Fig. 7. Electric conductivity of half-Heusler LiXZ alloys as a function of chemical potential calculated at different temperatures.

3.4. Thermoelectric properties

To illustrate that half-Heusler LiXZ ($X = \text{La}$, Y , and $\text{Y}=\text{Ge}$, Si) alloys are potential candidates for applications in thermoelectric generators, we have performed calculations for transport properties using semi-classical Boltzmann theory implemented in BoltzTraP code [38]. Fig. 6 shows the variation of Seebeck coefficient (S) as a function of chemical potential at temperatures; 300 K, 600 K and 800 K in the range, -0.6 eV– 1.2 eV. From Fig. 6, Seebeck coefficient has two peaks in both positive regions near VBM and negative regions near CBM, which indicates that either charge carrier holes or electrons can be involved in charge transport. Around the middle of bandgap on both sides, the value $S(\mu\text{V/K})$ rises with increasing chemical potential. For the good thermoelectric performance, the S coefficient should have a substantial value when the Fermi level enters the band edge [59]. The highest peaks of Seebeck (S) coefficient at 300 K near Fermi level are 1334 (-1252 $\mu\text{V/K}$), 1176 (-1068 $\mu\text{V/K}$), 1623 (-1547 $\mu\text{V/K}$) and 1449 (-1402 $\mu\text{V/K}$) p(n)-type for LiLaGe, LiLaSi, LiYGe, and LiYSi alloys, respectively. The concentration of holes or electrons causes σ/τ to increase with respect to temperature T in the region of bandgap, and then decreases away on both sides when hole or electron reaches its maximum concentration. Generally, the large value of PF is related to degenerated bands that are near Fermi level. This degeneracy increases the DOS with a low symmetry generated by d orbitals. Another factor that plays a crucial role in increasing PF is the flat and dispersive bands that we have

in these alloys.

From Fig. 6, it is noted that LiXZ ($X = \text{La}$, Ge , and $Z = \text{Ge}$, Si) exhibits p-type doping at ambient temperature at Fermi level. In addition, it is found that by raising the temperature, the maximum of S decreases considerably. However, the present results are consistent with previous calculations of I-III-IV half-Heusler alloys, which have a similar tendency as that reported by Naseri et al. [52] and Kamlesh et al. [29]. Figs. 7 and 8 show the variation of electronic thermal conductivity (κ_e/τ) and electrical conductivity (σ/τ) of LiXZ ($X = \text{La}, \text{Y}$ and $Z = \text{Si}, \text{Ge}$) alloys as a function of chemical potential in the temperature range, 300 K, 600 K and 800 K that conform to a comparable profile that the holes doping in half Heusler LiXZ ($X = \text{La}$) alloys will be valued for thermoelectric efficiency compared to electron doping. The thermal conductivity (κ/τ) consists of two parts, (κ_L/τ) lattice vibration part and (κ_e/τ) the electronic part, which is the unique part used by BoltzTraP code. For LiXZ ($X = \text{La}$), the hole carrier region and (σ/τ) are larger than electron carrier region. The opposite trend is observed for $X = \text{Yttrium}$ (Y). From Fig. 7 at room temperature, the higher values of conductivity are approximately $2.05 \times 10^{20} (\Omega\text{ms})^{-1}$ and $2.09 \times 10^{20} (\Omega\text{ms})^{-1}$ at 0.60 eV and 0.62 eV for LiLaGe and LiLaSi alloys, respectively, in the p-type region, n-type region takes the values, $2.61 \times 10^{20} (\Omega\text{ms})^{-1}$ and $2.69 \times 10^{20} (\Omega\text{ms})^{-1}$ at 1.89 eV and 1.79 eV, respectively.

The minor difference in (σ/τ) is suspected by the minor difference in their bandgaps. For n-type, Shrivastava et al. [59] have reported comparable higher values, which are $2.02 \times 10^{20} (\Omega\text{ ms})^{-1}$ and $2.04 \times 10^{20} (\Omega$

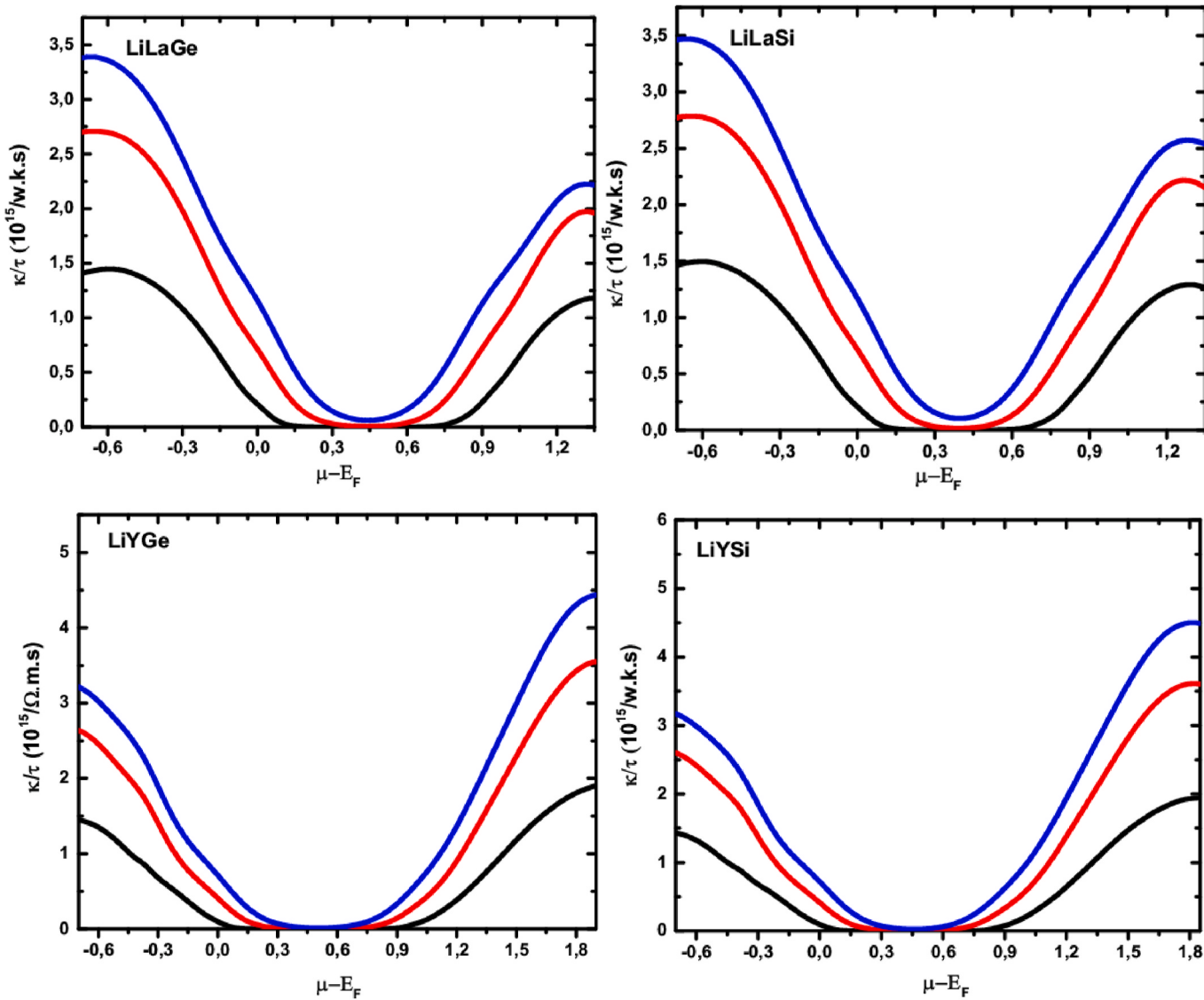


Fig. 8. Electric thermal conductivity of half-Heusler LiXZ alloys as a function of chemical potential calculated at different temperatures.

$\text{ms})^{-1}$ for KYSi and KYGe, while for p-type, slightly lower values are $2.09 \times 10^{20} (\Omega \text{ ms})^{-1}$ and $1.75 \times 10^{20} (\Omega \text{ ms})^{-1}$ for KLaSi and KLaGe, respectively as reported by Cherchab et al. [57]. Furthermore, the variation of (κ/τ) with (σ/τ) obeys Wiedemann-Franz Law [55], which stipulates that $\kappa = \sigma \cdot L \cdot T$, where L is Lorenz number. It is noted in Fig. 8 that minimum value of (κ_e/τ) is in chemical potential range, -0.3 and 0.9 eV for LiXZ ($X = \text{La}$) and between -0.3 and 1.2 eV for LiXZ ($X = \text{Y}$), which is present in the regions where the maximum performance of the investigated materials can be obtained in possible devices.

The lowest values of (κ_e/τ) at room temperature and chemical potential at -0.3 eV p (n-type) regions are $1.07 (0.22) \times 10^{15} (\text{W/Kms})$ $1.08 (0.48) \times 10^{15} (\text{W/Kms})$, $0.67 (0.025) \times 10^{15} (\text{W/Kms})$, and $0.74 (0.075) \times 10^{15} (\text{W/Kms})$ for LiLaGe, LiLaSi, LiLaGe, and LiLaSi alloys, respectively. The results of (κ_e/τ) are higher than reported by Citifi et al. [28] for KScX ($X = \text{C}$ and Ge) and Kamlesh et al. [29] for LiScX ($X = \text{Ge}$ and Si). At $\mu = E_F$ and room temperature, the values are $1.94 \times 10^{14} (\text{W/Kms})$, $1.9 \times 10^{14} (\text{W/Kms})$, $1.12 \times 10^{14} (\text{W/Kms})$ and $1.07 \times 10^{14} (\text{W/Kms})$ for LiLaGe, LiLaSi, LiLaGe, and LiLaSi alloys, respectively as compared with Shrivastava et al. [59], which are $1.48 \times 10^{14} (\text{W/Kms})$ and $1.36 \times 10^{14} (\text{W/Kms})$ for KScX ($X = \text{Sn}$ and Pb). However, Cherchab et al. [57] have reported using SOC effect that slightly lower values that are $1.3 \times 10^{14} (\text{W/Kms})$, $0.72 \times 10^{14} (\text{W/Kms})$, $0.62 \times 10^{14} (\text{W/Kms})$

and $0.36 \times 10^{14} (\text{W/Kms})$ for KLaSi, KLaGe, KLaSn and KLaC alloys, respectively. The efficiency of thermoelectrics is considered their figure of merit, which is given by $ZT = (S^2 \cdot \sigma \cdot T / \tau)$ in τ units.

The ZT of half-Heusler is approximately $\simeq 1$ in the temperature range, 500–1000 K [60–63]. Zhu et al. [63] have reported that half-Heusler LaPtSb alloys has high thermoelectric performance with ZT reaching 2.2 at 300 K, which exhibits very low thermal conductivity. ZT = 1.5 at 700 K for $\text{Ti}_{0.5}\text{Zr}_{0.25}\text{Hf}_{0.25}\text{NiSn}_{0.998}\text{Sb}_{0.002}$ that has been reported by Sakurada et al. [64], which is enhanced by Ti substitution on thermoelectric properties of half-Heusler (Zr,Hf)NiSn alloys. Fig. 9 shows the variation of ZT for LiXZ ($Z = \text{Si}, \text{Ge}$; $X = \text{Ge}, \text{La}$) alloys at room temperature. We have noted that ZT $\simeq 1$ in the vicinity of conduction and valence bands, showing comparable results to those found in K-half-Heusler and Li-half-Heusler-based alloys [28,29,52,52,65]. We have used mbj approach for all calculations, the increasing in temperature from 300 K to 800 K reduces the figure of merit for all alloys. Each one has two ZT peaks, one for n-type and other for p-type with same opposites values.

We note that total electronic conductivity curves are temperature sensitive, decrease with increasing the temperature. Hence, half-Heusler LiXZ alloys could be promising for thermoelectric applications. The power factor (PF), which is directly proportional to $S^2 \cdot \sigma$ in τ units, has

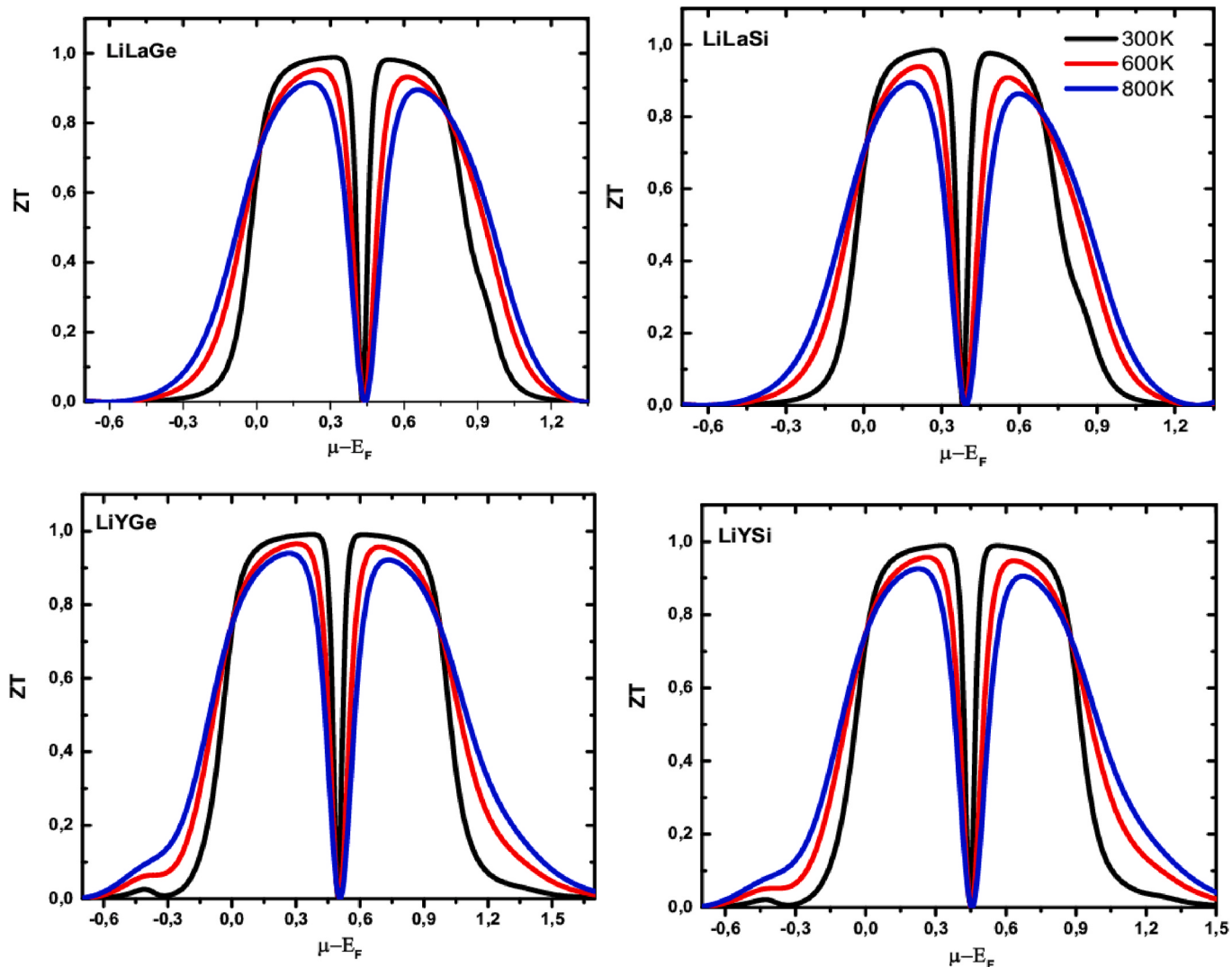


Fig. 9. Figure of merit (ZT) of half-Heusler LiXZ alloys as a function of chemical potential calculated at different temperatures.

also been calculated from a theoretical point of view. The optimal level of doping (concentrations of carrier) in which PF illustrates a maximum value helps to reduce doping experimentally [66]. Fig. 10(a) illustrates the variation of PF as a function of chemical potential of LiXZ ($X = La, Y$ and $Z = Ge, Si$) alloys at room temperature. It increases as chemical potential increases, which produces two peaks of PF, the highest one is for p-type doping region and another for n-type doping region in half-Heusler LiXZ alloys. The rapid increasing in DOS associated with the behaviour of band structure near VBM and CBM is the cause of higher value of power factor (PF) [67]. Fig. 10(b) illustrates the variation of PF with the carrier concentrations of LiXZ ($X = La, Y$ and $Z = Ge, Si$) alloys at room temperature. For LiXZ ($X = La$), the PF presents higher values for p-type concentration of $0.77 \times 10^{20} \text{ cm}^{-3}$ instead of electron concentration, which is $2.2 \times 10^{20} \text{ cm}^{-3}$. A similar trend seems to be for $X = Y$, and the maximum value of PF is $0.85 \times 10^{20} \text{ cm}^{-3}$ hole concentration, while for concentrations of electrons, it is $35-38 \times 10^{18} \text{ cm}^{-3}$. We can conclude that PF of LiXZ ($X = La$) is higher than LiXZ ($X = Y$). From the electronic band structure shown in the previous sections, we have noted that flat bands observed in LiXZ ($X = La$) rather than with $X = Y$ imply heavy effective mass, which ameliorates the power factor. Fig. 10(c) shows the variation of power factor as a function of temperature at Fermi level. The PF value decreases with temperature in half-Heusler LiXZ alloys, and these due to σ/τ . The maximum values of PF near fermi level at 300 K are $15 \times 10^{12} (\text{W/K}^2\text{ms})$, 12×10^{12}

($\text{W/K}^2\text{ms}$), $15.6 \times 10^{12} (\text{W/K}^2\text{ms})$ and $14.9 \times 10^{12} (\text{W/K}^2\text{ms})$ for LiLaGe, LiLaSi, LiYGe, and LiYSi alloys, respectively. The values of ZT are compared with others of half-Heusler that are close to unit [68–72].

3.5. Thermal conductivity

This work is based on the semi-empirical Debye-Callaway model. We have assumed that Umklapp diffusion is the dominant mechanism (see Ref. [73] for details). The total lattice thermal conductivity is given by equation (8) when $T > \theta_D$, phonon-phonon scattering dominates. The reduction in thermal conductivity κ_L leads to an improvement in ZT. It is well known that κ_L is very sensitive to variations in phonon dispersion, in another word, κ_L is sensitive to variations in the speed of sound inside the material. This leads to an analysis of thermal conductivity of phonon through Slack's equation [74–76].

$$\kappa_L = \frac{(6\pi^2)^{(2/3)} \bar{M}(V_s^3)}{(V)^{(2/3)} 4\pi^2 \gamma^2 T} = A \frac{\langle V_s^3 \rangle}{T} \quad (8)$$

$$A = \frac{2,4310^{-8}}{1 - \frac{0.514}{\gamma} + \frac{0.228}{\gamma^2}} \quad (9)$$

This relation is valid at high temperatures, $T > \theta_D$ [56,73]. We denote the average group velocity over the Brillouin zone as $\langle V_s^3 \rangle$ and we

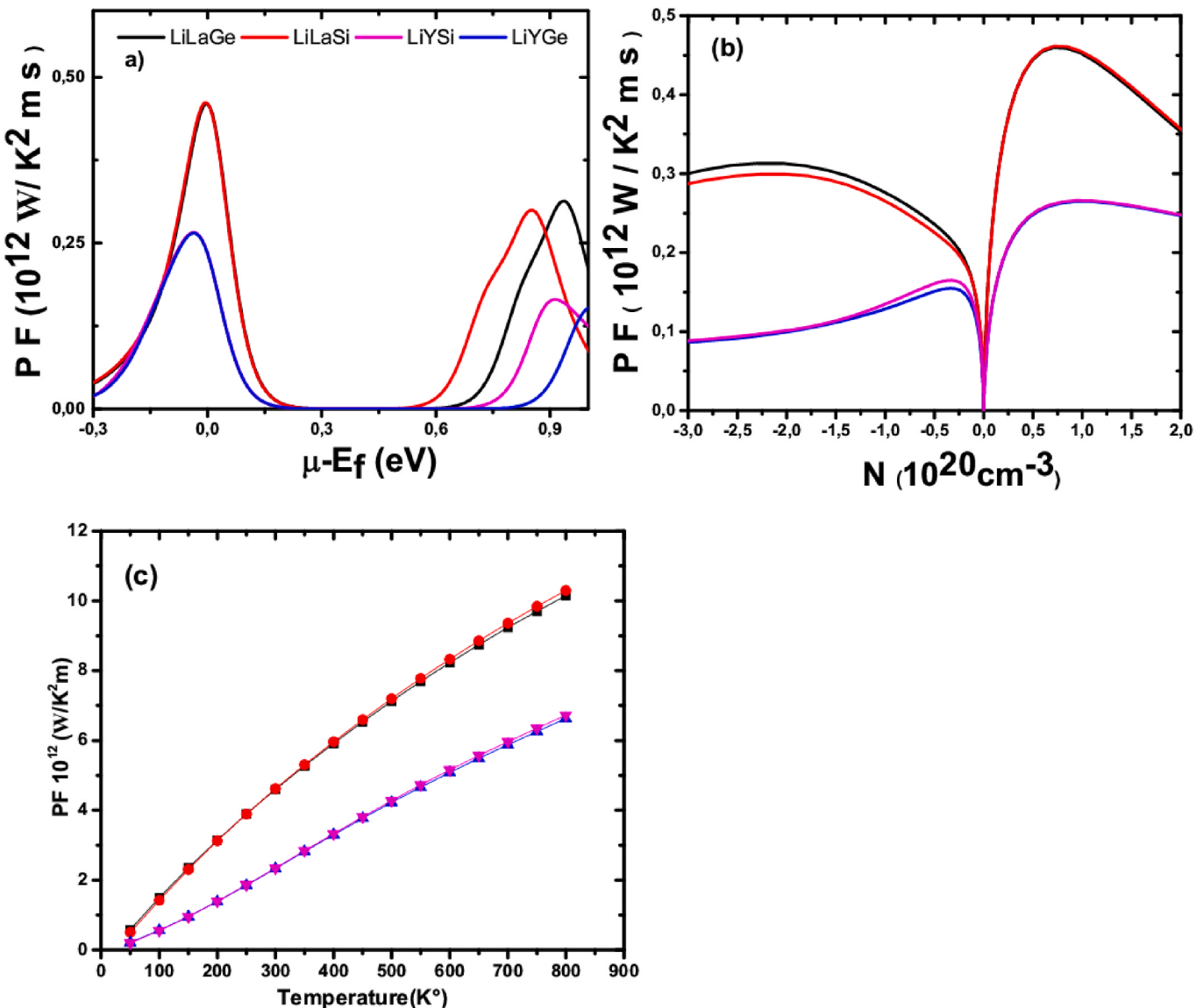


Fig. 10. Power factor of half-Heusler LiXZ alloys as function of a) carriers concentration b) chemical potential at room temperature c) temperatures.

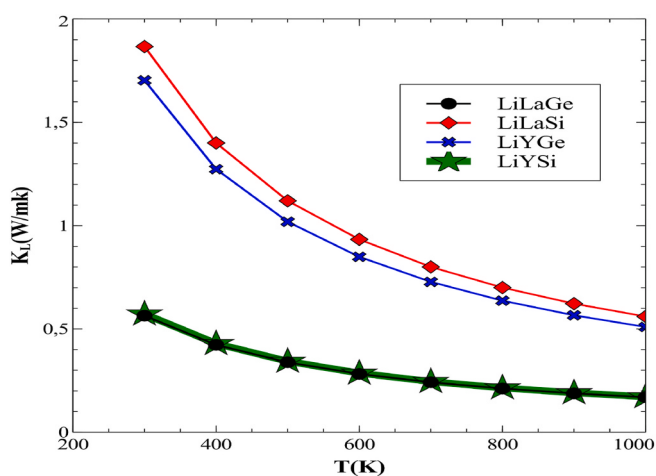


Fig. 11. Lattice thermal conductivity κ_L as a function of temperature for LiXZ ($X = \text{La}, \text{Y}$ and $Z = \text{Ge}, \text{Si}$) alloys.

consolidate \overline{M} an average atomic mass, V atomic volume and Grüneisen parameter γ into the coefficient A . In practice, A will be normalized to a pristine (control) sample and change in speed of sound will be used as an estimate for the change in average group velocity $\langle V_g^3 \rangle / \alpha \langle V_s^3 \rangle$. We have used Eq. (9) for normalize the coefficient A . This value is calculated for LiLaGe, LiLaSi and LiYGe alloys whereas V_s is the decisive parameter of model. Thus, since V_s is a measurable, there are no free parameters in this model when A is held constant [60,65]. The variation of κ_L as a function of temperature has been calculated and illustrated in Fig. 11. It can make a comparison between the four alloys. From the first view, we notice that, from the total thermal conductivity, the lattice thermal conductivity $\kappa_L = \kappa - \kappa_e$ of LiLaGe and LiYSi alloys take almost the same values. The values of LiLaGe and LiYSi at 300 K are close to PtLaSb (0.84 W/mk) [77], these values are favourable in the synthesize of thermoelectric alloys. The same remark is made for LiLaSi and LiYGe whose values of κ_L at 300 K are 1.7 w/mk and 1.9 w/mk, the two values are close to each other, where these values are decreasing to 0.6 w/mk at 1000 K. The general conclusion of these calculations show that these values are very small and do not influence κ_L , this is why the values of PF are almost the same.

4. Conclusions

In summary, the FP-LAPW method and semi-classical Boltzmann transport theory under the constant time relaxation have been used for investigating the structural, electronic, phonon dispersion and thermoelectric properties of novel half-Heusler LiXZ (X = La, Y, and Z = Ge, Si) (HH) Alloys. Our results have revealed that all alloys can be experimentally synthesized because they exhibit energetic, mechanical, and dynamic stability. Furthermore, the band structures of half-Heusler LiXZ alloys indicate a semiconducting nature with a direct bandgap, 0.974 eV (0.804 eV) for LiYGe (LiYSi) and indirect bandgap energies, 0.804 eV (0.704 eV) for LiLaGe (LiLaSi), with flatness occurring at the top of valence and bottom conduction bands. Our results have proved that these alloys exhibit a high figure of merit and power factor values at 300 K with low lattice thermal conductivity, especially for LaLiGe and LiYSi. κ_L decreases with an increasing in temperature due to increasing in Umpkapp processes that dominate the phonons scattering. Seebeck coefficients are higher than thermoelectric Bi₂Te₃. The obtained results show that half-Heusler (HH) LiXZ (X = La, Y, and Z = Ge, Si) alloys are a potential candidate for thermoelectric applications.

Funding

No funding was received.

Ethical approvals

We confirm that this work is original and has not been neither published elsewhere nor currently under consideration for publication elsewhere and has ethical issues and NO CONFLICT OF INTEREST.

Availability of data and materials

All used data is embedded in this manuscript and properly referenced where applicable.

CRediT authorship contribution statement

Hamid Missoum: Conceptualization. **Khedija Talbi:** Data curation. **Friha Khelfaoui:** Formal analysis. **Bachir Bouhadef:** Investigation. **Ali Mir:** Methodology. **Youcef Cherchab:** Software, Resources. **Rafael González-Hernández:** Writing – original draft, Validation. **Y. Al-Douri:** Writing – review & editing, Supervision.

Declaration of competing interest

The authors declare that they have no known competing financial interests or personal relationships that could have appeared to influence the work reported in this paper.

Data availability

No data was used for the research described in the article.

Acknowledgments

H.M., K.T., B.B., A.M., Y.C. would like to thank the General Directorate of Scientific Research and Technological Development “DGRSDT” and University of Relizane for their support.

References

- [1] M. Sajid, I. Hassan, A. Rahman, Energy Rev. 1 (2017) 78, 15.
- [2] R. Ahiska, H. Mamur, Int. J. Green Energy 13 (7) (2016) 672.
- [3] R. Ahiska, H. Mamur, IET Renew. Power Gener. 7 (6) (2013) 700.
- [4] Liuyijie Huang, Yihua Zheng, Luyi Xing, et al., Therm. Sci. Eng. Prog. (2023) 102064.
- [5] C. Bhowmik, S. Bhowmik, A. Ray, K.M. Pandey, Energy Rev. 1 (71) (2017) 796.
- [6] Osamu Yamashita, Shiochi Tomiyoshi, Ken et Makita, J. Appl. Phys. 93 (1) (2003) 368.
- [7] Yanzhong Pei, Aaron Lalonde, Shiro Iwanaga, et al., Energy Environ. Sci. 4 (6) (2011) 2085.
- [8] A. Zolriasatein, X. Yan, E. Bauer, et al., Mater. Des. 87 (2015) 883.
- [9] C. Han, Z. Li, S. Dou, Chin. Sci. Bull. 59 (2014) 2073.
- [10] G. Rogl, P.F. Rogl, Crystals 13 (7) (2023) 1152.
- [11] S. Chen, Z. Ren, Mater. Today 16387 (2013).
- [12] M. Gürth, G. Rogl, V.V. Romaka, A. Grytsiv, E. Bauer, P. Rogl, Acta Mater. 104 (2016) 210.
- [13] T. Zhu, C. Fu, X. Zhao, High figure of merit p-type FeNbHfSb thermoelectric material and the preparation method thereof, U. S. Patent US2018/0331268A1 (2018).
- [14] H. Zhu, J. Mao, Y. Li, J. Sun, Y. Wang, Q. Zhu, G. Li, Q. Song, J. Zhou, Y. Fu, et al., Nat. Commun. 10 (2019) 270.
- [15] J. Yu, C. Fu, Y. Liu, K. Xia, U. Aydemir, T.C. Chasapis, G.J. Snyder, X. Zhao, T. Zhu, Adv. Energy Mater. 8 (2017) 1701313.
- [16] G. Rogl, P. Sauerschnig, Z. Rykavets, V.V. Romaka, P. Heinrich, B. Hinterleitner, A. Grytsiv, E. Bauer, P. Rogl, Acta Mater. 131 (2017) 336.
- [17] H.B. Kang, B. Pourel, W. Li, H. Lee, U. Saparamadu, A. Nozariasbmarz, M. G. Kang, A. Gupta, J. Heremans, S. Priy, Mater. Today 36 (2020) 63.
- [18] J.P.A. Makongo, D.K. Misra, X.Y. Zhou, A. Pant, M.R. Shabetai, X.L. Su, C. Uher, K. L. Stokes, P.F.P. Poudeu, J. Am. Chem. Soc. 133 (2011) 18843.
- [19] J.P.A. Makongo, D.K. Misra, J.R. Salvador, N.J. Takas, G. Wang, M.R. Shabetai, A. Pant, P. Poudel, C. Uher, K.L. Stokes, et al., J. Solid State Chem. 184 (2011) 2948–2960.
- [20] J.E. Douglas, C.S. Birkel, M.-S. Miao, C.J. Torbet, G.D. Stucky, T.M. Pollock, R. Seshadri, Appl. Phys. Lett. 101 (2012) 183902.
- [21] N.S. Chauhan, S. Bathula, A. Vishwakarma, R. Bhardwaj, B. Gahtori, A. K. Srivastava, M. Saravanan, A.A. Dhar, Materialia 1 (2018) 168.
- [22] G. Rogl, M.J. Zehetbauer, P.F. Rogl, Mater. Trans. 60 (2019) 2071.
- [23] G. Rogl, S. Ghosh, L. Wang, J. Bursik, A. Grytsiv, R.C. Mallik, X.-Q. Chen, M. Zehetbauer, P. Rogl, Acta Mater. 183 (2020) 285.
- [24] B.S. Vikram, J. Kangsabani, A. Alam, J. Phys. Chem. Lett. 11 (15) (2020) 6364.
- [25] D.M. Hoat, M. Naseri, Chem. Phys. 528 (2020) 110510.
- [26] Y.O. Ciftci, S.D. Mahanti, J. Appl. Phys. 119 (2016) 145703.
- [27] D. Kieven, R. Klenk, S. Naghavi, C. Felser, T. Gruhn, Phys. Rev. B (2010) 81075208.
- [28] Y.O. Ciftci, M. Evecen, Ph. Transit 91 (2018) 1206.
- [29] P.K. Kamlesh, R. Gautam, S. Kumari, A.S. Verma, B. Physica, Condens. Matter 615 (2021) 412536.
- [30] A. Amudhavalli, R. Rajeswarapalanichamy, K. Iyakutti, A.K. Kushwaha, Comput. Cond. Mat 14 (2018) 55.
- [31] Binbin Jiang, et al., High-figure-of-merit and power generation in high-entropy GeTe-based thermoelectrics, Science 377 (2022) 208–213.
- [32] Omer Meroz, Nadav Elkabets, Yaniv Gelstein, Enhanced thermoelectric properties of n-type Bi₂Te₃-xSex alloys following melt-spinning, ACS Appl. Energy Mater. 3 (2020) 2090–2095.
- [33] Hang-Tian Liu, et al., High-performance in n-type PbTe-based thermoelectric materials achieved by synergistically dynamic doping and energy filtering, Nano Energy 91 (2022) 106706.
- [34] G. Komisarchik, et al., Solubility of Ti in thermoelectric PbTe compound, Intermetallics 89 (2017) 16–21.
- [35] Maor Kaller, David Fuks, Yaniv Gelstein, Sc solubility in p-type half Heusler (Ti_{1-x}Sc_x)NiSn thermoelectric alloys, J. Alloys Compd. 729 (2017) 446–452.
- [36] P. Blaha, K. Schwarz, G.K.H. Madsen, D. Kvánsíkka, J. Luitz, WIEN2k, an Augmented Plane Wave Plus Local Orbitals Program for Calculating Crystal Properties, Vienna University of Technology, Vienna, Austria, 2001.
- [37] P. Hohenberg, W. Kohn, Phys. Rev. 136 (1964) B864.
- [38] Allen B., Boltzmann Theory and Resistivity of Metals 1996 in: J.R. Chelikowsky, S. G. Louie (Eds.), Kluwer, Boston pp. 219.
- [39] J.P. Perdew, S. Burke, M. Ernzerhof, Phys. Rev. Lett. 77 (1996) 3865.
- [40] F. Tran, P. Blaha, K. Schwarz, J. Phys. Condens. Matter 19 (2007) 196208.
- [41] F. Tran, P. Blaha, Phys. Rev. Lett. 102 (2009) 226401.
- [42] A.D. Becke, E.R. Johnson, J. Chem. Phys. 124 (2012) 221101.
- [43] H.J. Monkhorst, J. Pack, D. Phys. Rev. B 13 (1976) 5188.
- [44] G.K. Madsen, D.J. Singh, Comput. Phys. Commun. 175 (2006) 67.
- [45] A. Togo, Tanaka, Scripta Mater. 108 (2015) 1.
- [46] F.D. Murnaghan, Proc. Natl. Acad. Sci. USA 30 (1944) 5390.
- [47] Z.A.A.R. Almaghosh, O. Arbouche, A. Dahani, A. Cherifi, M. Belabbas, A. Zenati, et al., Int. J. Thermophys. (2021) 421.
- [48] M.A. Jamal, Package for Calculating Elastic Tensors of Cubic Phases by Using Second-Order Derivative with Wien2k Package, 2013.
- [49] D.C. Wallace, in: Willey and Sons (Ltd.) Thermodynamics of Crystals, 1972.
- [50] Voigt W, Lehrbuch de Kristallphysik in Terubner, Leipzig (Eds.), 1928.
- [51] A. Reuss, Z. Angew. Math. Mech. 9 (1929) 49.
- [52] M.M. Naseri, D.M. Hoat, J. Mol. Graph. Model. 92 (2019) 249.
- [53] G. Wang, D. Wang, J. Alloys Compd. 682 375 (2016).
- [54] S. Pugh, London, Edinburgh Dublin Phil. Mag. J. Sci. 45 (1954) 823.
- [55] J. Zhang, H. Liu, L. Cheng, et al., Sci. Rep. 4 (2014) 6452.
- [56] G.A. Slack, S. Galganiatis, Phys. Rev. 133 (1A) (1964) A253.
- [57] Y. Cherchab, R. González-Hernández, Comput. Theor. Chem. 1200 (2021) 113231.
- [58] X.Q. Chen, H.Y. Niu, D.Z. Li, Y.Y. Li, Intermetallics 19 (2011) 1275.
- [59] D. Shrivastava, S.P. Sanyal, J. Alloys Compd. 784 (2019) 319.

- [60] S.A. Miller, P. Gorai, B.R. Ortiz, A. Goyal, D. Gao, S.A. Barnett, T.O. Mason, G. J. Snyder, Q. Lv, V. Stevanović, E.S. Toberer, *Chem. Mater.* 29 (2017) 6–2494.
- [61] W. Xie, A. Weidenkaff, X. Tang, Q. Zhang, J. Poon, T. Tritt, *Nanomaterials* 2 (2012) 379.
- [62] S. Chen, Z. Ren, *Mater. Today* 16 (2013) 387.
- [63] T. Zhu, C. Fu, H. Xie, Y. Liu, X. Zhao, *Adv. Energy Mater.* 5 (2015) 1500588.
- [64] Q.Y. Xue, H.J. Liu, D. Fan, L. Cheng, B.Y. Zhao, J. Shi, *Phys. Chem. Chem. Phys.* 181 (2016).
- [65] C. Toher, J.J. Plata, O. Levy, M. de Jong, M. Asta, M.B. Nardelli, S. Curtarolo, *Phys. Rev. B* 90 (2014) 17–174107.
- [66] S. Sakurada, N. Shutoh, *Appl. Phys. Lett.* 86 (2005) 082105.
- [67] F. Kong, Y. Hu, H. Hou, Y. Liu, B. Wang, L. Wang, *J. Solid State Chem.* 196 (2012) 5.
- [68] J. Yan, P. Gorai, B. Ortiz, S. Miller, S.A. Barnett, T. Mason, V. Stevanovic, E. S. Toberer, Material descriptors for predicting thermoelectric performance, *Energy Environ. Sci.* 8 (3) (2015) 983.
- [69] Fadila Belkharroubi, Walid Belkilali, Friha Khelfaoui, Fethi Boudahri, Mehdi Zahraoui, Nawal Belmiloud, kader bentayeb, El hadj Adel Abdellah, Radja Nour El Imene Bennoui, Raghd Belbachir, Y. Al-Douri, *Cryst. Res. Technol.* 59 (2024) 2300238.
- [70] G.S. AlGhamdi, A. Saini, A.A. AlShaikhi, R. Kumar, *J. Supercond. Nov. Magnetism* 35 (2021) 1–10.
- [71] A. Azouaoui, A. Harbi, M. Moutaabbid, A. Eddai, N. Benzakour, A. Rezzouk, *Indian J. Phys.* 97 (6) (2022) 172.
- [72] B. Rani, A.F. Wani, U.B. Sharopov, L. Patra, J. Singh, A.M. Ali, A.F. Abd El-Rehim, S.A. Khandy, S. Dhiman, K. Kaur, *Molecules* 27 (2022) 6567.
- [73] E.S. Toberer, A. Zevalkink, G.J. Snyder, *J. Mater. Chem.* 21 (2011) 40–15843.
- [74] M.D. Nielsen, V. Ozolins, J.P. Heremans, *Energy Environ. Sci.* 6 (2013) 570578.
- [75] D.T. Morelli, G.A. Slack, High lattice thermal conductivity Solids, in: *High Thermal Conductivity Materials*, Springer, New York,NY,USA, 2006, p. 37.
- [76] E.J. Skoug, J.D. Cain, D.T. Morelli, *Appl. Phys. Lett.* 96 (2010) 181905–181908.
- [77] Z. Feng, Y. Fu, Y. Zhang, D.J. Singh, *Phys. Rev. B* 101 (2020) 1.